PASJ: Publ. Astron. Soc. Japan **56**, 569–580, 2004 June 25

Critical Accretion Disk

Jun FUKUE
Astronomical Institute, Osaka Kyoiku University, Asahigaoka, Kashiwara, Osaka 582-8582
fukue@cc.osaka-kyoiku.ac.jp

(Received 2004 March 7; accepted 2004 April 8)

Abstract

For a supercritical accretion regime, we propose a *critical* accretion disk, where the mass-accretion rate is regulated just at the critical rate with the help of wind mass-loss. We first derive a critical radius, inside of which the standard picture is violated, using the condition that the radiative force is balanced by the gravity in the vertical direction. The critical radius $r_{\rm cr}$ is found to be $r_{\rm cr} = (9\sqrt{3}\sigma_{\rm T}/16\pi cm_{\rm p})\dot{M}_{\rm input} = 1.95(\dot{M}_{\rm input}/\dot{M}_{\rm crit})r_{\rm g}$, where $\dot{M}_{\rm input}$ is the mass-accretion rate at the outer edge of the disk, $\dot{M}_{\rm crit}$ the critical accretion rate, and $r_{\rm g}$ the Schwarzschild radius of the central object. Outside of this critical radius, the disk is in a radiation-pressure dominated standard state, while inside this radius the disk is in a critical state, where the excess mass is expelled by wind and the accretion rate is kept to be just at the critical rate at any radius inside $r_{\rm cr}$. In such a critical accretion disk, the disk thickness is $H \sim (1/6\sqrt{3})r$ and the surface temperature is $\sigma T^4 \sim (2/3\sqrt{3})L_{\rm E}/4\pi r^2$, where $L_{\rm E}$ is the Eddington luminosity. The total disk luminosity becomes $L_{\rm disk} \sim (2/3\sqrt{3})[\ln(r_{\rm cr}/r_{\rm in}) + 1]L_{\rm E}$, where $r_{\rm in}$ is the inner radius. We apply the present model to microquasars and narrow-line Seyfert 1 galaxies, which are supposed to be under supercritical accretion.

Key words: accretion, accretion disks — black hole physics — galaxies: active — microquasars — stars: winds, outflows — X-rays: stars

1. Introduction

Accretion disks are now widely believed to be energy sources in various active phenomena in the universe: in protoplanetary nebulae, in cataclysmic variables, in galactic X-ray binaries and microquasars, and in active galaxies and quasars. Accretion-disk models have been extensively studied during these three decades (see Kato et al. 1998 for a review).

From our present knowledge about the accretion-disk theory, there are three types of accretion disk models. The criterion is that the mass-accretion rate $\dot{M}$ in the disk around a central object of mass M is less or greater than the critical rate, defined by

$$\dot{M}_{\rm crit} \equiv \eta \dot{M}_{\rm E} \equiv \frac{L_{\rm E}}{c^2} = 1.39 \times 10^{17} \frac{M}{M_\odot}\ {\rm g\,s^{-1}}, \tag{1}$$

where $\dot{M}_{\rm crit}$ (= $L_{\rm E}/c^2$) is the *critical* accretion rate, $\dot{M}_{\rm E}$ (= $L_{\rm E}/\eta c^2$) the Eddington accretion rate, $L_{\rm E}$ (= $1.25 \times 10^{38} M/M_\odot$ erg s^{-1}) the Eddington luminosity, and η (~ 0.1) the efficiency.

For a subcritical accretion rate ($\dot{M} \leq \dot{M}_{\rm E}$), the disk is in the classical standard state (e.g., Shakura, Sunyaev 1973). For a very low accretion rate ($\dot{M} \ll \dot{M}_{\rm E}$), on the other hand, the disk is supposed to be in the optically-thin advection-dominated state, i.e., optically-thin ADAF (e.g., Ichimaru 1977; Narayan, Yi 1994; Abramowicz et al. 1995; Popham, Gammie 1998). Finally, for a supercritical accretion rate ($\dot{M} \gg \dot{M}_{\rm E}$), the disk must be in the optically-thick advection-dominated state, optically-thick ADAF or slim disk or supercritical disk (Abramowicz et al. 1988; Eggum et al. 1988; Szuszkiewicz et al. 1996; Beloborodov 1998; Watarai, Fukue 1999; Watarai et al. 2000; Mineshige et al. 2000; Fukue 2000; Kitabatake et al. 2002; Ohsuga et al. 2002, 2003; Watarai, Mineshige 2003).

In recent years, the final case of the disk in the supercritical accretion regime is of great interest, because such supercritical disks play important roles in various astronomical sites: in SS 433 and microquasars such as GRS 1915+105 and GRO J1655−40; in ultra-luminous X-ray sources; in super-soft X-ray sources; and in narrow-line Seyfert 1 galaxies and luminous quasars. Indeed, the spectral behavior of several black-hole binaries cannot be explained by the traditional standard disk, but is well reproduced by slim disk models (e.g., Kubota 2001).

Theoretically, however, there remains several unrevealed problems for disks under a supercritical accretion state. One of the question is whether the disk is entirely supercritical and geometrically thick, or not. In the spherical case, both the gravity and the radiation forces vary as r^{-2}, and the transition from the subcritical to supercritical regimes takes place in all space. In contrast to the spherical case, the supercritical condition in the disk system must be locally determined, since the gravity and radiation properties depend complicately on the distance r from the central object. Approximately speaking, the gravity varies as r^{-2}, but the radiation flux of the standard disk in the vertical direction varies as r^{-3}. Hence, the transition from the subcritical to supercritical regimes takes place at *some* radius, outside of which the disk is in the subcritical regime and maintains its shape under the dominant gravity, while inside the disk is in the supercritical regime and the standard state would be violated under the dominant radiation. Indeed, in numerical calculations (e.g., Watarai et al. 2000; Mineshige et al. 2000), it was empirically found that, inside some radius, the standard state is violated and the disk becomes an advection-dominated state.

Another question is whether the mass loss takes place or not,

and if it takes place, whether wind blows off in the entire disk or not. Active objects often exhibit mass loss in the form of winds and/or jets. Radiatively driven winds from accretion disks have been examined by several researchers (Bisnovatyi-Kogan, Blinnikov 1977; Katz 1980; Icke 1980, 1989; Melia, Königl 1989; Tajima, Fukue 1996, 1998; Watarai, Fukue 1999; Hirai, Fukue 2001). Since the surface temperature varies as a function of the radius, the radiation fields produced by the disk are very complicated. Using the calculated disk radiation fields, the radiatively-driven disk winds were examined by Icke (1980) without radiation drag, and by Tajima and Fukue (1998) including radiation drag. In the latter case, the wind does not blow off in the entire disk, but in the inner region, when the disk effective luminosity is of the order of unity. In addition, the configuration of radiatively-supported clouds above the disk was examined (Fukue 1996; Kitabatake, Fukue 2003); it was found that the cloud configuration becomes unstable above the inner disk when the disk effective luminosity exceeds about unity.

In this paper we thus examine supercritical accretion disks with wind mass-loss, more carefully than in previous studies (cf. Watarai, Fukue 1999; Fukue 2000; Kitabatake et al. 2002). We then propose a *critical accretion disk*, where the mass-accretion rate is regulated just at the critical rate with the help of the wind mass-loss.

In the next section we first derive a critical radius, inside of which the accretion disk is in a critical state. In section 3, a standard-like critical model is shown, while an advection-like critical model is presented in section 4. The general properties of critical accretion disks are discussed in section 5. In section 6 the present critical model is applied to microquasars and narrow-line Seyfert 1 galaxies. The final section is devoted to concluding remarks.

2. Critical Radius

In a spherically symmetric case, the supercritical condition was discussed by several researchers (Begelman 1979; King, Begelman 1999). They found that the luminosity generated by infall down to radius r will reach the Eddington limit at a radius of $R_{\rm ex} \sim (\dot{M}/\dot{M}_{\rm E}) r_{\rm g}$, where $r_{\rm g}$ is the Schwarzschild radius of the central object. This radius is also the *photon-trapping radius*.

Similar derivation in a global form would be also applied to the accretion-disk system. That is, from the condition that the luminosity of the standard-like disk down to radius r will reach the Eddington luminosity of the central object ($L_r = GM\dot{M}/2r = L_{\rm E} = 4\pi cGMm_{\rm p}/\sigma_{\rm T}$), we can determine some critical radius $r'_{\rm cr}$ as $r'_{\rm cr} = (\sigma_{\rm T}/8\pi cm_{\rm p})\dot{M}$. In the disk system, however, the gravity and radiation forces depend on the radius more complicately than those in the spherical case. Hence, we treat the problem more carefully, although the result does not alter very much.

Under the Newtonian approximation and using the cylindrical coordinates (r, φ, z), the local force balance in the vertical direction around the disk is expressed as

$$\text{Vertical Force} = -\frac{GMz}{R^3} + \frac{\sigma_{\rm T}}{m_{\rm p}c} F, \tag{2}$$

where $R = \sqrt{r^2 + z^2}$ and F is the radiative flux in the vertical direction. The gravitational force in the vertical direction becomes a maximum at $z_{\rm max} = (1/\sqrt{2})r$, and the maximum value of the vertical gravity is $-2GM/(3\sqrt{3}r^2)$. On the other hand, for the standard disk the radiative flux F in the vertical direction is $F = \sigma T^4 = 3GM\dot{M}/(8\pi r^3)$, where we drop the boundary correction factor $(1 - \sqrt{r_{\rm in}/r})$, $r_{\rm in}$ being the inner radius of the disk. Hence, the radiative force in the vertical direction becomes $3\sigma_{\rm T}GM\dot{M}/(8\pi m_{\rm p}cr^3)$.

Ultimately, we have a *critical radius* $r_{\rm cr}$, outside of which the radiation-pressure dominated standard disk is valid, and inside of which the radiative force overcomes the gravity and the traditional standard picture is violated:

$$r_{\rm cr} = \frac{9\sqrt{3}\sigma_{\rm T}}{16\pi m_{\rm p}c} \dot{M}_{\rm input}, \tag{3}$$

where the accretion rate $\dot{M}$ is replaced by the accretion rate $\dot{M}_{\rm input}$ at the outer edge of the disk. This critical radius is very similar to the spherical case (King, Begelman 1999), and depends only on $\dot{M}_{\rm input}$ and is independent of M. Numerically, this critical radius is

$$r_{\rm cr} = 5.71 \times 10^5 \frac{M}{M_\odot} \frac{\dot{M}_{\rm input}}{\dot{M}_{\rm crit}} \ {\rm cm} \tag{4}$$

or

$$r_{\rm cr} = \frac{9\sqrt{3}}{8} \dot{m} r_{\rm g} \sim 1.95 \dot{m} r_{\rm g}, \tag{5}$$

where $\dot{m} \equiv \dot{M}_{\rm input}/\dot{M}_{\rm crit}$ and $r_{\rm g} = 2GM/c^2$.

This final expression (5) clearly means that the entire disk would be in a supercritical state when the accretion rate is highly supercritical (e.g., $\dot{M}_{\rm input} \sim 10^5 \eta \dot{M}_{\rm E} \sim 10^5 \dot{M}_{\rm crit}$). In other words, when the accretion rate is moderately supercritical (e.g., $\dot{M}_{\rm input} \sim 10^{2-3} \dot{M}_{\rm crit}$), only the inner part of the disk is supercritical, while the outer part remains in a subcritical state. In addition, for an accretion disk around a black hole, this critical radius appears when the accretion rate exceeds the critical rate.

In numerical calculations (e.g., Watarai et al. 2000; Mineshige et al. 2000), it was shown that inside some radius (*transition* radius) the disk becomes an advection-dominated state. However, physical explanations concerning the existence of such a radius are insufficient, and therefore there is no analytical derivation of such a transition radius. The existence of the transition radius is also explained by the present formula (3). Indeed, in the calculation of Watarai et al. (2000) the transition radius is numerically located at around $100 r_{\rm g}$ for $\dot{m} = 100$; this value is very consistent with the present analytical result of the critical radius.

By the way, what is a *supercritical state* inside $r_{\rm cr}$? One extreme case is that the disk inside $r_{\rm cr}$ would be slim-disk like, where there is no mass loss and photon trapping takes place (Abramowicz et al. 1988; Szuszkiewicz et al. 1996; Fukue 2000; Watarai et al. 2000; Mineshige et al. 2000; Ohsuga et al. 2002; Watarai, Mineshige 2003). In this picture, "no-mass-loss" is only an assumption. Inside $r_{\rm cr}$, however, the radiation pressure force overcomes the gravity force, and mass loss would naturally take place. Observationally, moreover, there exists mass loss in various objects. Hence, another extreme case that we consider in this paper is that the disk inside $r_{\rm cr}$

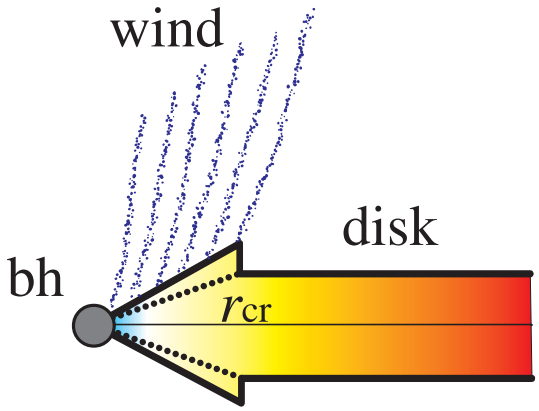

Fig. 1. Schematic picture of critical accretion disks. When the accretion rate at the outer edge of the disk is moderately supercritical, there exists some critical radius r_{cr}. Outside r_{cr}, the accretion rate is constant and the disk is a radiation-pressure dominated standard disk. Inside r_{cr}, the accretion rate decreases with the radius so as to maintain the critical rate, expelling any excess mass by the radiation-driven wind. The accretion rate must continuously change at r_{cr}, but other quantities, such as the disk thickness, would jump at r_{cr}, although there is no shock at r_{cr}.

would be highly mass-losing because of the radiation-pressure driven disk wind, as suggested in previous studies (Tajima, Fukue 1998; Kitabatake, Fukue 2003), and the accretion rate is regulated just at the critical rate (figure 1). This is the *critical accretion disk*.

In order for the inner disk to maintain the critical state, the mass-accretion rate satisfies the critical condition (3) at any given radius inside r_{cr}. That is, the accretion rate would vary as

$$\dot{M}(r) = \frac{16\pi c m_p}{9\sqrt{3}\sigma_T} r \tag{6}$$

inside r_{cr}. Thus, the wind mass-loss rate via radiatively-driven winds must be

$$\dot{M}_{wind} = \dot{M}_{input} - \dot{M}(r), \tag{7}$$

where $\dot{M}_{input}$ is the accretion rate at the outer edge of the disk (and at the critical radius).

It should be noted that, because of the advection motion in the inner critical disk, there may exist a jump in the physical quantities at a critical radius, as is schematically shown in figure 1.

In the subsequent sections we in turn examine a standard-like critical disk and an advection-like critical disk under condition (6).

3. Standard-Like Critical Accretion Disk

From a dynamical point of view, we first consider a standard-like critical accretion disk. For this case, we assume that, in the disk inside r_{cr}, the rotational velocity v_φ is nearly Keplerian v_K, and the viscous heating rate Q_{vis} is nearly equal to the radiative cooling rate Q_{rad}, and other quantities are all standard disk-like (Shakura, Sunyaev 1973; Kato et al. 1998), though the mass-accretion rate $\dot{M}$ decreases as in equation (6) at any given radius inside r_{cr}. We show several quantities below.

First, using the scale-height H of the disk in the radiation-pressure dominated region (Kato et al. 1998) and equation (6), we have a solution for H as

$$H = \begin{cases} \dfrac{3\kappa f_{in}}{32\pi c}\dot{M}_{input} & \text{for } r \geq r_{cr} \\ \dfrac{f_{in}}{6\sqrt{3}} r & \text{for } r \leq r_{cr}, \end{cases} \tag{8}$$

where κ is the electron-scattering opacity ($=\sigma_T/m_p$), and $f_{in} = 1 - \sqrt{r_{in}/r}$ is the boundary correction factor (this factor is set to be unity in this paper, although it is often retained explicitly). This solution means that the shape of the standard-like critical accretion disk is flat outside r_{cr}, and conical inside r_{cr} with some opening angle. In addition, the disk opening angle δ (defined by $H/r = \tan\delta$) is about $5.^\circ5$, and the disk is geometrically not so fat. It should be noted that the behavior of the inner solution ($H \propto r$) is the same as those for the advection-like critical disk discussed in the next section. The coefficient becomes the same when the parameter $\sqrt{c_3}$, introduced in the next section (see also the appendix), is 0.096 ($\delta = 5.^\circ5$).

Similarly, replacing the accretion rate by equation (6), we have a solution for the effective temperature T_{eff} as

$$\sigma T_{eff}^4 = \begin{cases} \dfrac{3GM\dot{M}_{input}}{8\pi r^3} f_{in} & \text{for } r \geq r_{cr} \\ \dfrac{2}{3\sqrt{3}} \dfrac{L_E}{4\pi r^2} f_{in} & \text{for } r \leq r_{cr}, \end{cases} \tag{9}$$

where L_E is the Eddington luminosity ($=4\pi cGM/\kappa$). It should be noted that the behavior of the inner solution ($\sigma T_{eff}^4 \propto r^{-2}$) is the same as those for the advection-like critical disk discussed in the next section. The coefficient becomes the same when the parameter $\sqrt{c_3}$, introduced in the next section (see also the appendix), is 0.5132 ($\delta = 27^\circ$).

The optical depth τ is

$$\tau = \begin{cases} \dfrac{256\pi c^2}{9\alpha\kappa\dot{M}_{input} f_{in}} \sqrt{\dfrac{r^3}{GM}} \\ \quad = \dfrac{128\sqrt{2}}{9\alpha f_{in}} \dfrac{L_E}{\dot{M}_{input} c^2} \sqrt{\dfrac{r^3}{r_g^3}} & \text{for } r \geq r_{cr} \\ \dfrac{16\sqrt{6}}{\alpha f_{in}} \sqrt{\dfrac{r}{r_g}} & \text{for } r \leq r_{cr}. \end{cases} \tag{10}$$

This means that, in spite of wind mass-loss, the disk is sufficiently optically thick for electron scattering in an inner critical region as well as in an outer standard region.

Finally, the radial drift velocity v_r is

$$-v_r = \begin{cases} \dfrac{9\alpha\kappa^2\dot{M}_{input}^2 f_{in}}{1024\pi^2 c^2} \sqrt{\dfrac{GM}{r^5}} & \text{for } r \geq r_{cr} \\ \dfrac{\alpha f_{in}}{108} \sqrt{\dfrac{GM}{r}} & \text{for } r \leq r_{cr}. \end{cases} \tag{11}$$

That is, the radial drift velocity in an inner critical region is proportional to the Keplerian velocity.

In standard-like critical accretion disks, the physical quantities of an outer standard disk, such as H, T_{eff}, τ, and v_r, are *continuously* connected with those of an inner critical disk at

the critical radius $r_{\rm cr}$ (see dashed curves in figure 1 and figures for applications).

4. Advection-Like Critical Accretion Disk

We next consider an advection-like critical accretion disk. In this case, we assume that, in the disk inside $r_{\rm cr}$, the advection cooling rate $Q_{\rm adv}$ is not negligible, and of the order of the viscous heating rate $Q_{\rm vis}$ and the radiative cooling rate $Q_{\rm rad}$, while the rotational velocity v_φ is generally somewhat smaller than the Keplerian speed $v_{\rm K}$. For optically-thick supercritical disks, self-similar solutions without mass loss were found by Watarai and Fukue (1999) and Fukue (2000), and those with mass loss by Kitabatake, Fukue, and Matsumoto (2002). As a solution for the inner advection-like critical disk, we use the latter self-similar solutions with mass loss, which are summarized in the appendix. Because of the critical condition (6), we have imposed, for the inner critical disk, that the mass-accretion rate should vary as $\dot{M} \propto r$; therefore, the parameter s in the appendix is fixed as $s = 1/2$.

Using the scale-height H of the disk in the radiation-pressure dominated region (Kato et al. 1998) and self-similar solutions for optically-thick supercritical disks with mass loss (appendix), we have a solution for H as

$$H = \begin{cases} \dfrac{3\kappa f_{\rm in}}{32\pi c}\dot{M}_{\rm input} & \text{for } r \geq r_{\rm cr} \\ \sqrt{c_3}\, r & \text{for } r \leq r_{\rm cr}, \end{cases} \tag{12}$$

where c_3 is a numerical factor of the order of unity, and determined by the specific heat ratio γ, the viscous parameter α, and the advection fraction f (see appendix). As is known from equation (12), this numerical factor is related to the disk opening angle δ by

$$\sqrt{c_3} = H/r = \tan\delta. \tag{13}$$

This solution means that the shape of the advection-like critical accretion disk is flat outside $r_{\rm cr}$, and conical inside $r_{\rm cr}$ with some opening angle. It should be noted that the scale-heights of the inner and outer disks are smoothly connected at $r_{\rm cr}$ when the parameter $\sqrt{c_3}$ is 0.096 ($\delta = 5.^\circ5$). When $\sqrt{c_3}$ is larger (smaller) than 0.096, the scale-height of the inner disk is larger (smaller) than that of the outer disk at $r_{\rm cr}$ (cf. figure 1). In many cases of the advective solutions, a significant fraction of the viscous heating is transferred to the advection cooling ($\sqrt{c_3} \sim 1$), and the scale-height of the inner disk becomes thicker at $r_{\rm cr}$.

A solution for the effective temperature $T_{\rm eff}$ is expressed as

$$\sigma T_{\rm eff}^4 = \begin{cases} \dfrac{3GM\dot{M}_{\rm input}}{8\pi r^3} f_{\rm in} & \text{for } r \geq r_{\rm cr} \\ \dfrac{3}{4}\sqrt{c_3}\dfrac{L_{\rm E}}{4\pi r^2} & \text{for } r \leq r_{\rm cr}. \end{cases} \tag{14}$$

In the inner critical region, the temperature varies as $T_{\rm eff} \propto r^{-1/2}$. It should be noted that the value of the effective temperature is continuous at $r_{\rm cr}$ when the parameter $\sqrt{c_3}$ is 0.5132 ($\delta = 27^\circ$), and discontinuous when the parameter is not.

The optical depth τ is

$$\tau = \begin{cases} \dfrac{256\pi c^2}{9\alpha\kappa\dot{M}_{\rm input} f_{\rm in}}\sqrt{\dfrac{r^3}{GM}} \\ \quad = \dfrac{128\sqrt{2}}{9\alpha f_{\rm in}}\dfrac{L_{\rm E}}{\dot{M}_{\rm input}c^2}\sqrt{\dfrac{r^3}{r_{\rm g}^3}} & \text{for } r \geq r_{\rm cr} \\ \dfrac{16\sqrt{6}}{\alpha f_{\rm in}}\sqrt{\dfrac{r}{r_{\rm g}}} & \text{for } r \leq r_{\rm cr}. \end{cases} \tag{15}$$

This means that, in spite of wind mass-loss, the disk is sufficiently optically thick for electron scattering in an inner critical region as well as in an outer standard region. It should be noted that, in the advection-like critical accretion disk, the optical depth (and therefore, the surface density Σ) can be smoothly connected at $r_{\rm cr}$.

The radial velocity v_r is

$$-v_r = \begin{cases} \dfrac{9\alpha\kappa^2\dot{M}_{\rm input}^2 f_{\rm in}}{1024\pi^2c^2}\sqrt{\dfrac{GM}{r^5}} & \text{for } r \geq r_{\rm cr} \\ c_1\alpha\sqrt{\dfrac{GM}{r}} & \text{for } r \leq r_{\rm cr}. \end{cases} \tag{16}$$

That is, the radial drift velocity in an inner critical region is proportional to the Keplerian velocity. It should be noted that the radial velocity is continuous at $r_{\rm cr}$ when the parameter c_1 is $1/108$, and discontinuous when the parameter is not.

Finally, the azimuthal velocity v_φ is

$$v_\varphi = \begin{cases} \sqrt{\dfrac{GM}{r}} & \text{for } r \geq r_{\rm cr} \\ c_2\sqrt{\dfrac{GM}{r}} & \text{for } r \leq r_{\rm cr}. \end{cases} \tag{17}$$

It should be noted that the azimuthal velocity of the inner disk generally becomes smaller than that of the outer disk at $r_{\rm cr}$, since the parameter c_2 is somewhat smaller than unity (advection motion).

In advection-like critical accretion disks, physical quantities, such as H, $T_{\rm eff}$, τ, and v_r, generally jump at the critical radius $r_{\rm cr}$ (see solid curves in figure 1 and figures for applications). This is because a part of the viscous heating is converted into an internal energy and an advection energy.

5. General Properties of Critical Accretion Disks

In the previous two sections we show solutions of critical accretion disks with winds for two simple cases: standard-like and advection-like cases. Thanks to the critical condition (6), both solutions are very similar, except for numerical factors. In this section we discuss the general properties of critical accretion disks.

5.1. Accretion Rates

For the present critical accretion disk, from the critical condition (6), the mass-accretion rate $\dot{M}$ is expressed as

$$\dot{M} = \begin{cases} \dot{M}_{\rm input} & \text{for } r \geq r_{\rm cr} \\ \dfrac{16\pi c m_{\rm p}}{9\sqrt{3}\sigma_{\rm T}} r = \dot{M}_{\rm input}\dfrac{r}{r_{\rm cr}} & \text{for } r \leq r_{\rm cr}. \end{cases} \tag{18}$$

Hence, the mass-accretion rate $\dot{M}_{\rm in}$ at the inner edge of the disk is

$$\dot{M}_{\rm in} = \dot{M}_{\rm input}\frac{r_{\rm in}}{r_{\rm cr}} = 0.51\frac{L_{\rm E}}{c^2}\frac{r_{\rm in}}{r_{\rm g}}. \tag{19}$$

This means that the mass-accretion rate $\dot{M}_{\rm in}$ at the inner edge of the critical accretion disk is always of the order of $L_{\rm E}/c^2 = \dot{M}_{\rm crit}$, provided that the inner radius $r_{\rm in}$ is around $r_{\rm g}$, whereas the mass-accretion rate $\dot{M}_{\rm input}$ at the outer edge can highly exceed the critical rate $\dot{M}_{\rm crit}$.

Using the above mass-accretion rate (18), the mass-loss rate per unit surface area must be

$$2\dot{\rho}H = -\frac{1}{2\pi r}\frac{d\dot{M}}{dr} = \begin{cases} 0 & \text{for } r \geq r_{\rm cr} \\ -\dfrac{\dot{M}_{\rm input}}{2\pi r_{\rm cr}}\dfrac{1}{r} & \text{for } r \leq r_{\rm cr}. \end{cases} \tag{20}$$

The total wind mass-loss rate $\dot{M}_{\rm wind}$ is evaluated as

$$\dot{M}_{\rm wind} = \dot{M}_{\rm input}\left(1 - \frac{r_{\rm in}}{r_{\rm cr}}\right). \tag{21}$$

5.2. Black-Hole Growth Rate

If the central object is a black hole of mass M, it grows via mass accretion. We can easily evaluate the growth rate (growing time) of the black hole using the mass-accretion rate.

When the mass-accretion rate at the outer edge is smaller than the critical rate, the mass-accretion rate at the inner edge is equal to that at the outer edge, and the black-hole mass grows linearly as

$$M = M_0 + \dot{M}_{\rm input}t, \tag{22}$$

where M_0 is the initial mass. In this case the growth time $\tau_{\rm growth}$ is $M_0/\dot{M}_{\rm input}$.

When the mass-accretion rate at the outer edge exceeds the critical rate, on the other hand, the accretion rate at the inner edge is suppressed, as in equation (19). In this case the black-hole mass is determined by

$$\frac{dM}{dt} = \dot{M}_{\rm in} = 0.51\frac{L_{\rm E}}{Mc^2}\frac{r_{\rm in}}{r_{\rm g}}M. \tag{23}$$

Hence, the black-hole mass exponentially grows as

$$M = M_0 e^{t/\tau_{\rm growth}}, \tag{24}$$

where the growth time is expressed as

$$\tau_{\rm growth} = \frac{1}{0.51}\frac{Mc^2}{L_{\rm E}}\frac{r_{\rm g}}{r_{\rm in}} = 3.0\times10^8\frac{3\,r_{\rm g}}{r_{\rm in}}\ {\rm yr}. \tag{25}$$

This timescale is about the Eddington timescale, which is the growth timescale of a black hole under the Eddington rate.

5.3. Optical Depth

As already shown in equations (10) and (15), the optical depth for electron scattering is sufficiently larger than unity in the outer standard region as well as in the inner critical region.

When we consider both electron scattering and free-free absorption, the opacity becomes

$$\overline{\kappa} = \kappa_{\rm es} + \kappa_{\rm ff} = 0.4 + 6.4\times10^{22}\rho T^{-3.5}\ {\rm cm^2\,g^{-1}} \tag{26}$$

for pure hydrogen plasmas. In this case, the effective optical depth τ_* is defined (Kato et al. 1998) by

$$\tau_* \equiv \sqrt{\kappa_{\rm es}\kappa_{\rm ff}}\rho H \tag{27}$$

for accretion disks.

For the present critical disk, this effective optical depth is calculated for a standard-like critical disk as

$$\tau_* = \begin{cases} 8.44\times10^{-3}\alpha^{-17/16}m^{-1/16}\dot{m}^{-2}f_{\rm in}^{-2}(r/r_{\rm g})^{93/32} \\ \qquad \text{for } r \geq r_{\rm cr} \\ 3.22\times10^{-2}\alpha^{-17/16}m^{-1/16}f_{\rm in}^{-2}(r/r_{\rm g})^{29/32} \\ \qquad \text{for } r \leq r_{\rm cr}, \end{cases} \tag{28}$$

where $m = M/M_\odot$ and $\dot{m} = \dot{M}_{\rm input}/\dot{M}_{\rm crit}$. Hence, similar to the case of the standard accretion disk, the effective optical depth is small in the inner region of the disk.

5.4. Disk Luminosity

Using the surface temperature distributions (9) and (14), we can roughly estimate the total luminosity emitted from the disk:

$$\begin{aligned} L_{\rm disk} &= \int_{r_{\rm in}}^{r_{\rm cr}} 2\sigma T_{\rm eff}^4 2\pi r\,dr + \int_{r_{\rm cr}}^{\infty} 2\sigma T_{\rm eff}^4 2\pi r\,dr \\ &= \left\{ \begin{array}{c} \dfrac{2}{3\sqrt{3}} \\ \dfrac{3}{4}\sqrt{c_3} \end{array} \right\} L_{\rm E}\ln\frac{r_{\rm cr}}{r_{\rm in}} + \frac{2}{3\sqrt{3}}L_{\rm E}, \end{aligned} \tag{29}$$

where the first term is the luminosity from the inner critical disk, the second one is that from the outer standard disk, and the critical radius $r_{\rm cr}$ is assumed to be sufficiently larger than the inner radius $r_{\rm in}$. Moreover, in the first term the upper factor in the bracket means the case of the standard-like critical disk, while the lower factor means the advection-like disk, respectively. Similar to usual supercritical disks without mass loss, a part of generated energy via accretion is carried by accreting gas and trapped photons into a black hole, instead being radiated away. As a result, the total disk luminosity is suppressed at the order of the Eddington luminosity, $L_{\rm disk} \sim L_{\rm E}$.

In terms of expression (5), this total luminosity is further rewritten as

$$L_{\rm disk} = \frac{2}{3\sqrt{3}}\left[\left\{ \begin{array}{c} 1 \\ \dfrac{9\sqrt{3}}{8}\sqrt{c_3} \end{array} \right\}\ln\left(\frac{1.95}{r_{\rm in}/r_{\rm g}}\dot{m}\right) + 1\right]L_{\rm E}. \tag{30}$$

This relation (30) under a supercritical rate is very similar to the case of the usual supercritical accretion disks (e.g., Watarai, Fukue 1999; Watarai et al. 2000), when the accretion rate is sufficiently higher than the critical rate ($\dot{m} = \dot{M}_{\rm input}c^2/L_{\rm E} \gg 1$). Indeed, Watarai et al. (2000) derived a similar expression by a numerical calculation. The present analytical expression (30) is very consistent with the result by Watarai et al. (2000) within a factor of 3 for $\dot{m} \gg 1$ (the present case is less than their case).

5.5. Continuum Spectrum

For the present purpose, we assume that the disk surface radiates blackbody radiation B_ν with temperature $T_{\rm eff}(r)$. Then, the continuum spectrum (luminosity per frequency) L_ν can be calculated (see, e.g., Kato et al. 1998) by

$$L_\nu = 2\int_{r_{\rm in}}^{r_{\rm out}} \pi B_\nu(r) 2\pi r\, dr, \tag{31}$$

where a factor 2 means both sides of the disk, and

$$B_\nu(r) = \frac{2h}{c^2}\frac{\nu^3}{e^{h\nu/k_{\rm B}T_{\rm eff}(r)}-1}. \tag{32}$$

For the present critical accretion disk, the surface temperature is expressed as [equation (9) or (14)]

$$T_{\rm eff} = \begin{cases} T_{\rm cr}(r/r_{\rm cr})^{-p_1} & \text{for } r_{\rm in} \le r \le r_{\rm cr} \\ T_{\rm cr}(r/r_{\rm cr})^{-p_2} & \text{for } r_{\rm cr} \le r \le r_{\rm out}, \end{cases} \tag{33}$$

where $p_1 = 1/2$, $p_2 = 3/4$, and $T_{\rm cr}$ the temperature at $r_{\rm cr}$. Hence, the continuum spectrum (31) is written as

$$L_\nu = 2\pi\frac{4\pi h}{c^2}\frac{r_{\rm cr}^2}{p_1}\left(\frac{k_{\rm B}T_{\rm cr}}{h\nu}\right)^{2/p_1}\nu^3\int_{x_{\rm in}}^{x_{\rm cr}}\frac{x^{2/p_1}-1}{e^x-1}\,dx + 2\pi\frac{4\pi h}{c^2}\frac{r_{\rm cr}^2}{p_2}\left(\frac{k_{\rm B}T_{\rm cr}}{h\nu}\right)^{2/p_2}\nu^3\int_{x_{\rm cr}}^{x_{\rm out}}\frac{x^{2/p_2}-1}{e^x-1}\,dx, \tag{34}$$

where

$$x_{\rm in} = \frac{h\nu}{k_{\rm B}T_{\rm cr}}\left(\frac{r_{\rm in}}{r_{\rm cr}}\right)^{p_1}, \tag{35}$$

$$x_{\rm cr} = \frac{h\nu}{k_{\rm B}T_{\rm cr}}, \tag{36}$$

$$x_{\rm out} = \frac{h\nu}{k_{\rm B}T_{\rm cr}}\left(\frac{r_{\rm out}}{r_{\rm cr}}\right)^{p_2}. \tag{37}$$

As can be seen from equation (34), the slope of the continuum breaks at $h\nu \sim k_{\rm B}T_{\rm cr}$. In the low-frequency part, where radiation from the outer standard disk is dominant, the slope becomes $\nu L_\nu \propto \nu^{4-2/p_2} = \nu^{4/3}$, which is just that of the standard disk. On the other hand, in the high-frequency part, where radiation from the inner critical disk is dominant, the slope is $\nu L_\nu \propto \nu^{4-2/p_1} = \nu^0$, which is just that of the supercritical disk. For the standard-like critical disk, the surface temperature $T_{\rm cr}$ at the critical radius becomes

$$T_{\rm cr} = 2.13\times10^7\left(\frac{M}{M_\odot}\right)^{-1/4}\left(\frac{\dot M}{\dot M_{\rm crit}}\right)^{-1/2}\ {\rm K}, \tag{38}$$

and the break energy at the spectrum is

$$h\nu_{\rm cr} \sim k_{\rm B}T_{\rm cr} = 1.84\left(\frac{M}{M_\odot}\right)^{-1/4}\left(\frac{\dot M}{\dot M_{\rm crit}}\right)^{-1/2}\ {\rm keV}. \tag{39}$$

As was already stated, in the present critical disk with mass loss, there exists a break in the slope of the surface temperature distribution at $r = r_{\rm cr}$. This nature may be common in the case of supercritical disks with or without mass loss. That is, in general there are *two* different slopes in the surface temperature distribution as well as in the continuum spectrum for supercritical and/or critical accretion disks. However, in the reduction of observational data or in the numerical fitting (e.g., Watarai et al. 2000; Mineshige et al. 2000), it has often been used a mean value p of the slope. In order to treat the problem precisely, we should use two values p_1 and p_2 for fittings.

6. Applications

In this section we apply the present model of critical accretion disks to several active astronomical objects, including an accretion disk around a black hole, which are supposed to be under supercritical accretion: microquasars and narrow-line Seyfert 1 galaxies.

6.1. Microquasars

Microquasars are highly luminous galactic X-ray sources with mildly relativistic jets, such as SS 433, Cyg X-3, and (maybe) 1E 1740.7−2942, or with highly relativistic superluminal jets, such as GRS 1915+105 and GRO J1655−40 (Mirabel, Rodríguez 1998). These microquasars are now supposed to be stellar-mass black holes under supercritical accretion (e.g., Watarai et al. 2000; Watarai, Mineshige 2003). We thus apply the present critical disk to microquasars.

As typical values for microquasars, we adopt

$$M = 10M_\odot M_1, \tag{40}$$

$$\dot M_{\rm input} = 10^{-6}\,M_\odot\ {\rm yr}^{-1}\dot M_{-6}, \tag{41}$$

where $M_1 = M/(10M_\odot)$ and $\dot M_{-6} = \dot M_{\rm input}/(10^{-6}\,M_\odot\ {\rm yr}^{-1})$. Therefore, the Schwarzschild radius is $r_{\rm g} = 3\times10^6 M_1$ cm, the Eddington luminosity $L_{\rm E} = 1.25\times10^{39}\,M_1\ {\rm erg\,s^{-1}}$, and the critical accretion rate $\dot M_{\rm crit} = 2.21\times10^{-8}\,M_1 M_\odot\ {\rm yr}^{-1}$ (i.e., $\dot m \sim 100$). In this case the critical radius is located at

$$r_{\rm cr} = 2.59\times10^8\dot M_{-6}\ {\rm cm}, \tag{42}$$

$$= 5.71\times10^6 M_1\dot m\ {\rm cm}, \tag{43}$$

which is $\sim 100 r_{\rm g}$.

For the case of a standard-like critical disk, several physical quantities of critical accretion disks in microquasars are numerically

$$H = \begin{cases} 2.51\times10^7\dot M_{-6}\ {\rm cm} & \text{for } r \ge r_{\rm cr} \\ 0.96\times10^5 r_6\ {\rm cm} & \text{for } r \le r_{\rm cr}, \end{cases} \tag{44}$$

$$T_{\rm eff} = \begin{cases} 1.15\times10^8 M_1^{1/4}\dot M_{-6}^{1/4} r_6^{-3/4}\ {\rm K} & \text{for } r \ge r_{\rm cr} \\ 2.87\times10^7 M_1^{1/4} r_6^{-1/2}\ {\rm K} & \text{for } r \le r_{\rm cr}, \end{cases} \tag{45}$$

$$-v_r = \begin{cases} 2.29\times10^{13}\alpha M_1^{1/2}\dot M_{-6}^2 r_6^{-5/2}\ {\rm cm\,s^{-1}} \\ \qquad \text{for } r \ge r_{\rm cr} \\ 3.37\times10^8\alpha M_1^{1/2} r_6^{-1/2}\ {\rm cm\,s^{-1}} \\ \qquad \text{for } r \le r_{\rm cr}. \end{cases} \tag{46}$$

where $r_6 = r/(10^6\,{\rm cm})$. These standard-like solutions as well as several advection-like ones are plotted in figure 2.

In figure 2 several physical quantities of critical accretion disks in microquasars are shown as a function of the radius (in units of $r_{\rm g}$): i.e., (a) scale-height H in units of $r_{\rm g}$, (b) surface temperature $T_{\rm eff}$, and (c) radial drift velocity $-v_r$. As can be easily seen in figure 2, for a typical microquasar the critical radius $r_{\rm cr}$ is located at around $100 r_{\rm g}$. Outside $r_{\rm cr}$ accretion disks are in a radiation-pressure dominated standard state, while inside $r_{\rm cr}$, we suppose, disks are in a critical accretion state, where the mass-accretion rate is regulated just at the critical rate via wind mass-loss. For such critical accretion disks, we consider two types: one is a standard-like critical disk (dashed

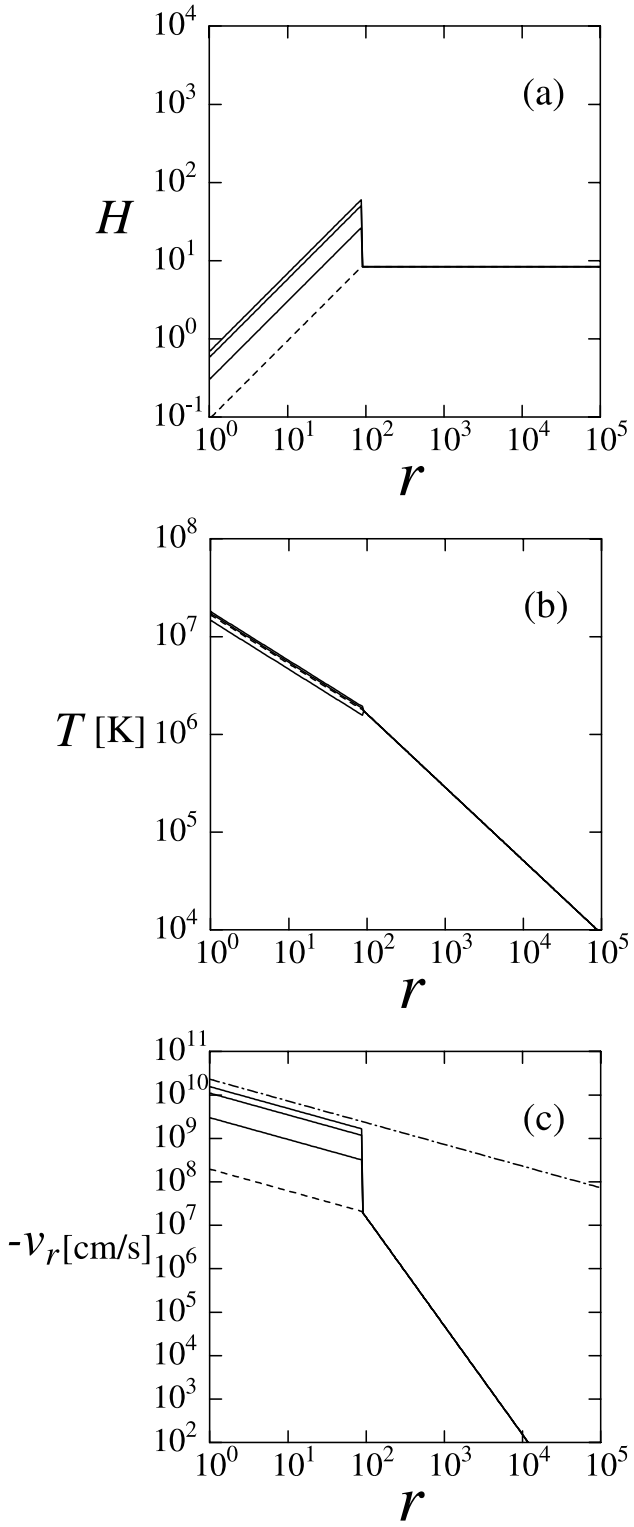

Fig. 2. Critical accretion disks in microquasars as a function of the radius (in units of r_g). The ordinates are (a) scale-height H in units of r_g, (b) surface temperature $T_{\rm eff}$, and (c) radial drift velocity $-v_r$. Outside the critical radius $r_{\rm cr}$ accretion disks are in a radiation-pressure dominated standard state, while for a disk inside $r_{\rm cr}$ we consider two types of critical accretion disks: one is a standard-like critical disk (dashed curve), and the other is an advection-like critical disk (solid curve). In the latter case, as an example, the parameter is $\gamma = 4/3$, $\alpha = 1$, and $f = 0.1$, 0.5, and 1 from the lower line to the upper line. A chain-dotted line in (c) means the Keplerian velocity.

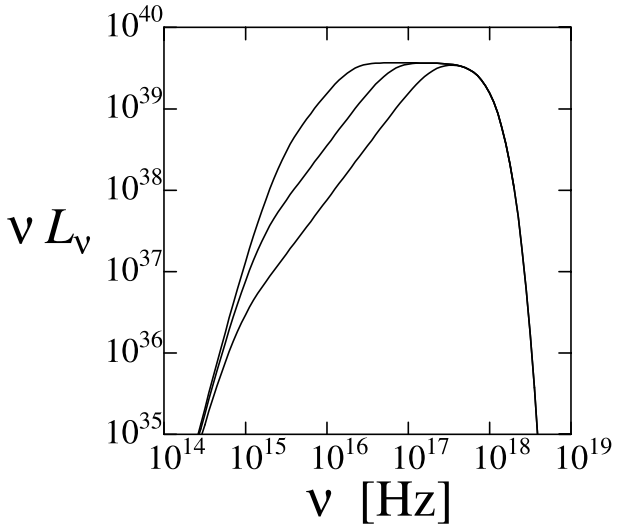

Fig. 3. Continuum spectra of critical accretion disks in microquasars. The central black-hole mass is fixed as $10M_\odot$, while the mass accretion-rate is $10^{-6}\,M_\odot$ yr^{-1}, $10^{-5}\,M_\odot$ yr^{-1}, and $10^{-4}\,M_\odot$ yr^{-1}, from bottom to top.

curve), and the other is an advection-like critical disk (solid curve). In the latter case, as an example, the parameter is $\gamma = 4/3$, $\alpha = 1$, and $f = 0.1$, 0.5, and 1 from a lower line to an upper line. A chain-dotted line in (c) means the Keplerian velocity.

As can be seen in figure 2, and already stated, in the standard-like critical disk physical quantities are smoothly connected at $r_{\rm cr}$, while this is not generally the case in the advection-like critical disk. For example, the scale-height thickens and the radial drift velocity approaches the Keplerian speed as f increases (figures 2a and 2c).

The emergent spectra are shown in figure 3 for the case of a standard-like critical disk. The central black-hole mass is fixed as $10M_\odot$, while the mass accretion-rate is $10^{-6}\,M_\odot$ yr^{-1}, $10^{-5}\,M_\odot$ yr^{-1}, and $10^{-4}\,M_\odot$ yr^{-1}, from bottom to top. As can be seen in figure 3, there exists a break in the continuum spectrum. In addition, the maximum of νL_ν is always of the order of the Eddington luminosity.

Recently, Kubota (2001) examined a microquasar XTE J1550−564 through a spectral analysis. She found that the temperature slope p shifts from 3/4 to 1/2 when its luminosity slightly exceeds the Eddington luminosity. This result is supposed to be evidence for a slim disk. As is well known, there exists high mass loss in microquasars. Hence, under the present picture, Kubota's result may be reconsidered so that the inner critical region extends with, e.g., an increase of the accretion rate.

6.2. *Narrow-Line Seyfert 1 Galaxies*

Narrow-line Seyfert 1 galaxies have relatively narrow Balmer-lines compared with those of a typical Seyfert 1, while the other properties are similar to those of Seyfert 1 (e.g., Boller et al. 1996). They exhibit extreme soft X-ray excess and large variability in soft X-rays. These narrow-line Seyfert 1 galaxies are supposed to contain relatively less massive black holes

($\sim 10^{5-6} M_\odot$) under supercritical accretion (e.g., Mineshige et al. 2000). We thus apply the present critical disk to narrow-line Seyfert 1 galaxies.

As typical values for narrow-line Seyfert 1 galaxies, we adopt

$$M = 10^6 M_\odot M_6, \tag{47}$$

$$\dot{M}_{\rm input} = 1\, M_\odot\ {\rm yr}^{-1} \dot{M}_0, \tag{48}$$

where $M_6 = M/(10^6 M_\odot)$ and $\dot{M}_0 = \dot{M}_{\rm input}/(1\ M_\odot\ {\rm yr}^{-1})$. Therefore, the Schwarzschild radius is $r_{\rm g} = 3 \times 10^{11} M_6$ cm, the Eddington luminosity $L_{\rm E} = 1.25 \times 10^{44} M_6\ {\rm erg\,s^{-1}}$, and the critical accretion rate $\dot{M}_{\rm crit} = 2.21 \times 10^{-3}\, M_6\, M_\odot\ {\rm yr}^{-1}$ (i.e., $\dot{m} \sim 1000$). In this case, the critical radius is located at

$$r_{\rm cr} = 2.59 \times 10^{14} \dot{M}_0\ {\rm cm}, \tag{49}$$

$$= 5.71 \times 10^{11} M_6 \dot{m}\ {\rm cm}, \tag{50}$$

which is $\sim 1000 r_{\rm g}$.

For the case of a standard-like critical disk, several physical quantities of critical accretion disks in narrow-line Seyfert 1 galaxies are numerically

$$H = \begin{cases} 2.51 \times 10^{13} \dot{M}_0\ {\rm cm} & \text{for } r \geq r_{\rm cr} \\ 0.96 \times 10^{10} r_{11}\ {\rm cm} & \text{for } r \leq r_{\rm cr}, \end{cases} \tag{51}$$

$$T_{\rm eff} = \begin{cases} 1.15 \times 10^7 M_6^{1/4} \dot{M}_0^{1/4} r_{11}^{-3/4}\ {\rm K} & \text{for } r \geq r_{\rm cr} \\ 1.61 \times 10^6 M_6^{1/4} r_{11}^{-1/2}\ {\rm K} & \text{for } r \leq r_{\rm cr}, \end{cases} \tag{52}$$

$$-v_r = \begin{cases} 2.29 \times 10^{15} \alpha M_6^{1/2} \dot{M}_0^2 r_{11}^{-5/2}\ {\rm cm\,s^{-1}} \\ \qquad \text{for } r \geq r_{\rm cr} \\ 3.37 \times 10^8 \alpha M_6^{1/2} r_{11}^{-1/2}\ {\rm cm\,s^{-1}} \\ \qquad \text{for } r \leq r_{\rm cr}. \end{cases} \tag{53}$$

where $r_{11} = r/(10^{11}\,{\rm cm})$. These standard-like solutions as well as several advection-like ones are plotted in figure 4.

In figure 4, several physical quantities of critical accretion disks in narrow-line Seyfert 1 galaxies are shown as a function of the radius (in units of $r_{\rm g}$): i.e., (a) scale-height H in units of $r_{\rm g}$, (b) surface temperature $T_{\rm eff}$, and (c) radial drift velocity $-v_r$. As can be easily seen in figure 4, for typical narrow-line Seyfert 1 galaxies the critical radius $r_{\rm cr}$ is located at around $1000 r_{\rm g}$. Outside $r_{\rm cr}$ accretion disks are in a radiation-pressure dominated standard state, while inside $r_{\rm cr}$, we suppose, disks are in a critical accretion state, where the mass-accretion rate is regulated just at the critical rate via wind mass-loss. For such critical accretion disks, we consider two types: one is a standard-like critical disk (dashed curve), and the other is an advection-like critical disk (solid curve). In the latter case, as an example, the parameter is $\gamma = 4/3$, $\alpha = 1$, and $f = 0.1$, 0.5, and 1 from a lower line to an upper line. A chain-dotted line in (c) means the Keplerian velocity.

As can be seen in figure 4, and already stated, in the standard-like critical disk the physical quantities are smoothly connected at $r_{\rm cr}$, while this is not generally the case in the advection-like critical disk. For example, the scale-height thickens and the radial drift velocity approaches the Keplerian speed as f increases (figures 4a and 4c).

The emergent spectra are shown in figure 5 for the case of a standard-like critical disk. The central black-hole mass is

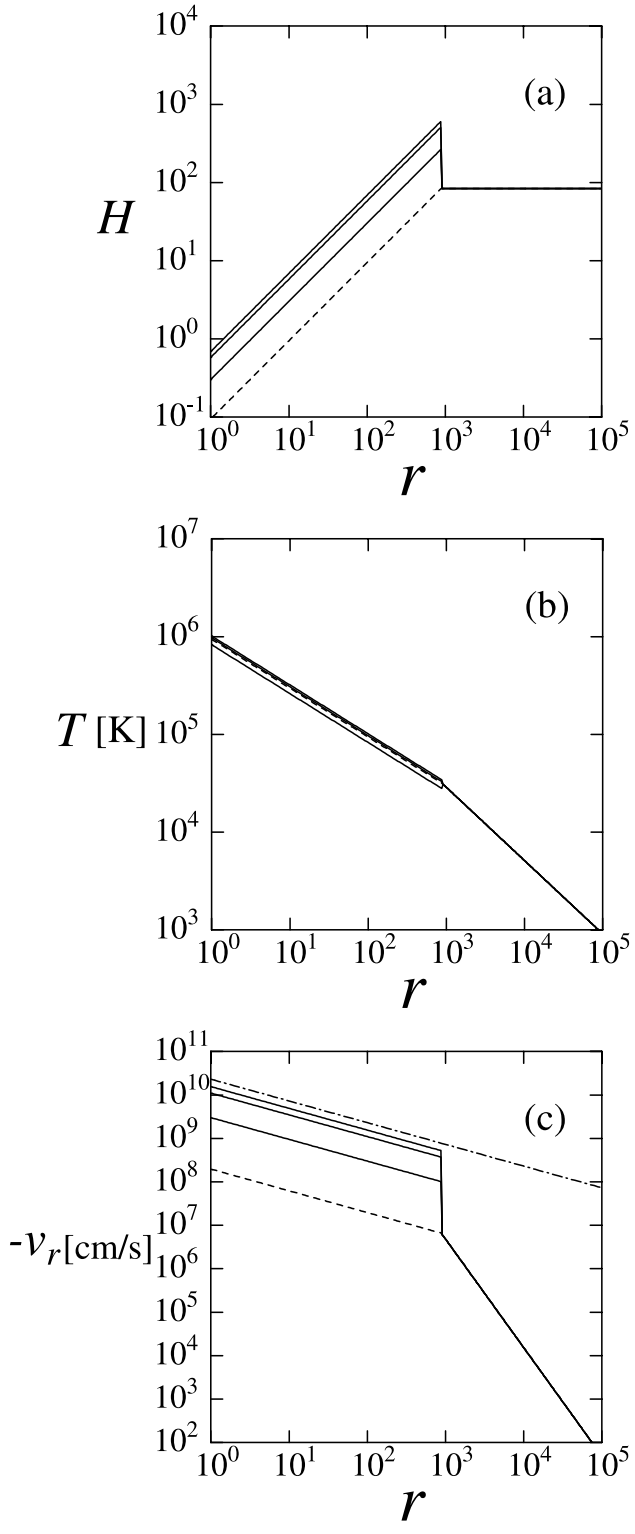

Fig. 4. Critical accretion disks in narrow-line Seyfert 1 galaxies as a function of the radius (in units of $r_{\rm g}$). The ordinates are (a) scale-height H in units of $r_{\rm g}$, (b) surface temperature $T_{\rm eff}$, and (c) radial drift velocity $-v_r$. Outside the critical radius $r_{\rm cr}$ accretion disks are in a radiation-pressure dominated standard state, while for a disk inside $r_{\rm cr}$ we consider two types of critical accretion disks: one is a standard-like critical disk (dashed curve), and the other is an advection-like critical disk (solid curve). In the latter case, as an example, the parameter is $\gamma = 4/3$, $\alpha = 1$, and $f = 0.1$, 0.5, and 1 from the lower line to the upper line. A chain-dotted line in (c) means the Keplerian velocity.

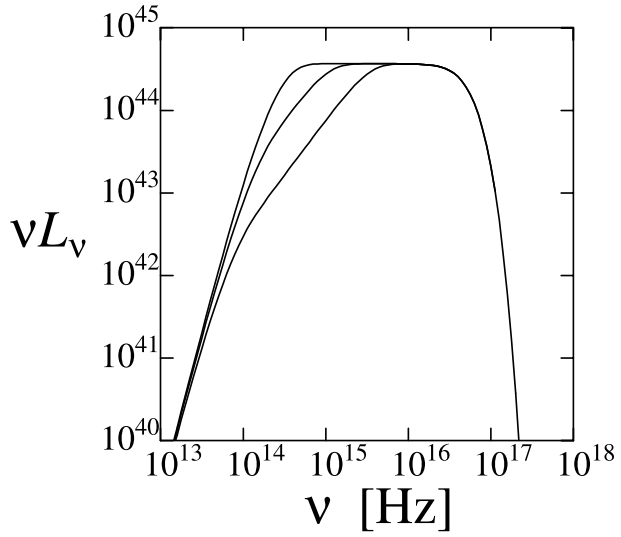

Fig. 5. Continuum spectra of critical accretion disks in narrow-line Seyfert 1 galaxies. The central black-hole mass is fixed as $10^6 M_\odot$, while the mass accretion-rate is $1\,M_\odot$ yr^{-1}, $10\,M_\odot$ yr^{-1}, and $100\,M_\odot$ yr^{-1}, from bottom to top.

fixed as $10^6\,M_\odot$, while the mass accretion-rate is $1\,M_\odot$ yr^{-1}, $10\,M_\odot$ yr^{-1}, and $100\,M_\odot$ yr^{-1}, from bottom to top. As can be seen in figure 5, there exists a break in the continuum spectrum. In addition, the maximum of νL_ν is always of the order of the Eddington luminosity.

7. Concluding Remarks

In this paper we proposed a *critical accretion disk*, where the mass-accretion rate is regulated just at the critical rate via the wind mass-loss, inside some critical radius. We have analytically derived the critical radius and other physical quantities of critical accretion disks.

1. The critical radius $r_{\rm cr}$ is found to be $r_{\rm cr} = (9\sqrt{3}\sigma_{\rm T}/16\pi cm_{\rm p})\dot{M}_{\rm input} = 1.95(\dot{M}_{\rm input}/\dot{M}_{\rm crit})r_{\rm g}$, where $\dot{M}_{\rm input}$ is the mass-accretion rate at the outer edge of the disk, $\dot{M}_{\rm crit}$ the critical accretion rate, and $r_{\rm g}$ the Schwarzschild radius of the central object.
2. Outside this critical radius, the disk is in a radiation-pressure dominated standard state with constant thickness (H = constant), while inside the critical radius the disk is in a critical state with conical shape, like $H \sim (1/6\sqrt{3})r$.
3. The radial distribution of the surface temperature $T_{\rm eff}$ changes its slope at $r_{\rm cr}$: $T_{\rm eff} \propto r^{-3/4}$ at $r \geq r_{\rm cr}$ and $T_{\rm eff} \propto r^{-1/2}$ at $r \leq r_{\rm cr}$. In addition, the surface temperature $T_{\rm cr}$ at the critical radius is $T_{\rm cr} = 2.13 \times 10^7 (M/M_\odot)^{-1/4}(\dot{M}/\dot{M}_{\rm crit})^{-1/2}$ K.
4. The radial infall velocity v_r also changes its pattern at $r_{\rm cr}$: $v_r \propto r^{-5/2}$ at $r \geq r_{\rm cr}$ and $v_r \propto r^{-1/2}$ at $r \leq r_{\rm cr}$.
5. The disk is sufficiently optically thick for electron scattering on both sides of the critical radius, whereas the effective optical depth is small in the inner region.
6. The emergent spectra L_ν of the critical accretion disk have a break at some frequency $\nu_{\rm cr}$: $\nu L_\nu \propto \nu^{4/3}$ in the low frequency part and $\nu L_\nu \propto \nu^0$ in the high frequency part. The break energy is $h\nu_{\rm cr} \sim k_{\rm B}T_{\rm cr} = 1.84(M/M_\odot)^{-1/4}(\dot{M}/\dot{M}_{\rm crit})^{-1/2}$ keV.
7. The total disk luminosity is found to be $L_{\rm disk} \sim (2/3\sqrt{3})[\ln(r_{\rm cr}/r_{\rm in}) + 1]L_{\rm E}$, where $r_{\rm in}$ is the inner radius.

We further apply the present critical accretion disk to micro-quasars and narrow-line Seyfert 1 galaxies, which are supposed to be under supercritical accretion.

There are two extreme possibilities for a disk state inside the critical radius: one is the traditional supercritical disk without any mass loss, and the other is the present critical disk with mass loss. Although the realistic situation would lie between these two extremes, observational facts of winds/jets support the mass loss. In any case, the *mass-loss rate* is one main parameter that determines the disk state inside the critical radius. The amount of the mass-loss rate would be determined by the momentum deposition from photon to the gas within unit time. If, however, there is an advection motion via viscosity, the radial drift motion would influence the mass-loss rate so as to reduce it.

In addition, for critical accretion disks, we examined two minor versions: standard-like critical disks and advection-like critical disks. As can be seen from the figures in the applications, advection-like critical disks approach standard-like critical disks as the advection fraction f becomes small. In other words, the *advection fraction* is another main parameter that determines the structure of critical accretion disks. In the present luminous case the advection fraction involves the effect of photon trapping (e.g., Ohsuga et al. 2002, 2003). Hence, the amount of the advection fraction would be determined by the energy transfer rate in the radial and vertical directions: some part of energy is advected inward via photon trapping to be swallowed by a black hole, while some part is transferred upward via photon diffusion to escape, although some part is transferred inward via diffusion to infall. Moreover, in the realistic situation, the advection fraction may depend on both the radius and the height. In order to evaluate the advection fraction quantitatively, the disk structure must be solved under radiation hydrodynamics.

The present critical disk would give a new aspect on the accretion disk model, in spite of its simpleness. In its application, however, there remain several points that must be considered with caution. First, the present critical accretion disk has some geometrical thickness, similar to supercritical accretion disks. Because of the geometrical thickness, several effects appear, including a projection effect, self-occultation, self-irradiation, and so on (see Fukue 2000 for the case of supercritical disks). For example, due to self-occultation, the disk luminosity decreases and the high energy part of the spectrum drops when we see a disk with a sufficiently high inclination angle. Second, since the present treatment is self-similar, the boundary effect at the innermost region was not correctly included. Moreover, we also neglected the relativistic effect, which would be important at the innermost region. Thirdly, within the framework of the analytical models, we treat the critical radius as some discontinuity, although it is

not a shock. More realistically, the outer standard disk would smoothly connect to the inner critical disk at the critical radius. Finally, the stability of the present critical disk and other time-dependent behavior are left as future work.

This work has been supported in part by a Grant-in-Aid for Scientific Research (15540235 JF) of the Ministry of Education, Culture, Sports, Science and Technology.

Appendix. Supercritical Accretion Disks with Winds

In this appendix we describe a model of a supercritical accretion disk, where a significant fraction of the accreting gas is expelled as a superwind, under a self-similar treatment (Watarai, Fukue 1999; Fukue 2000; Kitabatake et al. 2002).

A.1. Basic Equations

Let us suppose a gaseous disk rotating around and infalling onto a central object of mass M. The disk is assumed to be steady and axisymmetric. Although the disk is not infinitesimally thin, but has a finite thickness, the physical quantities are assumed to depend only on the radius r, and vertically integrated equations are used.

Hence, the continuity equation integrated in the vertical direction is expressed for the present purpose as

$$\frac{1}{r}\frac{d}{dr}(r\Sigma v_r) = 2\dot{\rho}H, \tag{A1}$$

where Σ is the disk surface density, v_r the radial velocity, $\dot{\rho}$ the mass-loss rate per unit volume, and H the disk half-thickness.

The momentum equation is

$$v_r\frac{dv_r}{dr} = \frac{v_\varphi^2}{r} - \frac{GM}{r^2} - \frac{1}{\rho}\frac{d}{dr}\left(\rho c_s^2\right), \tag{A2}$$

where v_φ is the rotation velocity and c_s is the sound speed, which is defined as $c_s^2 \equiv p/\rho$, p being the pressure. There is no net momentum gain/loss associated with the wind.

The angular momentum conservation is

$$r\Sigma v_r\frac{d}{dr}\left(rv_\varphi\right) = \frac{d}{dr}\left(\frac{2\alpha\rho c_s^2 r^3 H}{\Omega_K}\frac{d\Omega}{dr}\right), \tag{A3}$$

where α is the viscous parameter, $\Omega\,(=v_\varphi/r)$ the angular speed, and Ω_K the Keplerian angular speed. There is no net angular-momentum gain/loss associated with the wind.

The hydrostatic balance in the vertical direction is

$$\frac{GM}{r^3}H^2 = \frac{\Pi}{\Sigma} = c_s^2, \tag{A4}$$

where Π is the vertically integrated pressure. There is no net momentum gain/loss in the vertical direction associated with the wind. Furthermore, we assume that the wind initial velocity as well as the advection motion in the vertical direction is sufficiently small, compared with the sound speed.

The energy equation becomes

$$\frac{\Sigma v_r}{\gamma-1}\frac{dc_s^2}{dr} + 2Hc_s^2\left(\dot{\rho} - v_r\frac{d\rho}{dr}\right) = f\frac{\alpha\Sigma c_s^2 r^2}{\Omega_K}\left(\frac{d\Omega}{dr}\right)^2, \tag{A5}$$

where $\rho\ (=\Sigma/2H)$ is the gas density and f is an advection parameter. That is to say, the advection heating Q_{adv} is assumed to be expressed by the viscous heating Q_{vis} as $Q_{adv} = Q_{vis} - Q_{rad} = fQ_{vis}$, Q_{rad} being the radiative cooling (Narayan, Yi 1994). In this energy equation (A5), the term associated with mass loss on the left-hand-side comes from the work done by pressure with the help of the continuity equation (A1).

A.2. Self-Similar Solutions

Although the simple self-similar model cannot describe the innermost region and outer limb, it well reproduces the overall structures in a non-relativistic regime. In the self-similar model the velocities are assumed to be expressed as follows:

$$v_r(r) = -c_1\alpha v_K(r), \tag{A6}$$

$$v_\varphi(r) = c_2 v_K(r), \tag{A7}$$

$$c_s^2(r) = c_3 v_K^2(r), \tag{A8}$$

where

$$v_K(r) = \sqrt{\frac{GM}{r}}, \tag{A9}$$

and constants c_1, c_2, and c_3 are determined later.

From the hydrostatic equation (A4), we obtain the disk half-thickness H as

$$H/r = \sqrt{c_3} = \tan\delta. \tag{A10}$$

Hence, a supercritical disk with winds also has a conical surface, whose opening (half-thickness) angle is δ.

Assuming the surface density Σ to be in the form of

$$\Sigma = \Sigma_0 r^s, \tag{A11}$$

we obtain, e.g.,

$$\Pi = \Sigma c_s^2 = \Sigma_0 c_3 r^s\frac{GM}{r}. \tag{A12}$$

It should be noted that, for a self-similar disk without any wind mass-loss, the suffix s is $s = -1/2$. On the other hand, for a critical accretion disk in the present paper, the suffix s is $s = 1/2$, because of the restriction of a critical accretion rate (6).

Then, from the momentum, angular momentum, and energy equations [(A2), (A3), and (A5)], we can determine the constants uniquely as follows:

$$c_1 = \frac{1}{3\alpha^2}h(\alpha,\epsilon'), \tag{A13}$$

$$c_2^2 = \frac{2\epsilon'}{9\alpha^2}h(\alpha,\epsilon'), \tag{A14}$$

$$c_3 = \frac{2}{9\alpha^2}h(\alpha,\epsilon'), \tag{A15}$$

where

$$\epsilon' = \frac{1}{f}\left(\frac{5/3-\gamma}{\gamma-1}\right), \tag{A16}$$

$$h(\alpha,\epsilon') \equiv \sqrt{\left(\frac{2-s}{s+1}+2\epsilon'\right)^2 + 18\alpha^2} - \left(\frac{2-s}{s+1}+2\epsilon'\right). \tag{A17}$$

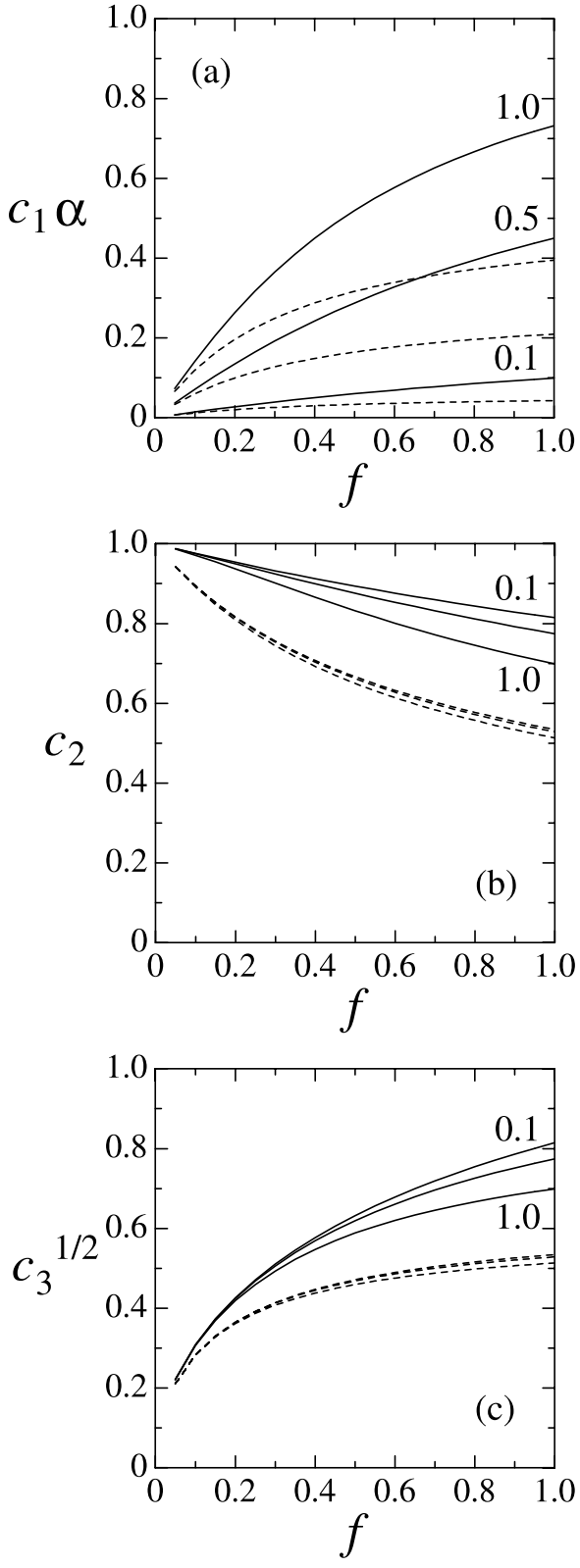

Fig. 6. Numerical factors c_i's as a function of the advection parameter f for several values of the viscous parameter α: (a) $c_1\alpha$ ($= -v_r/v_K$), (b) c_2 ($= v_\varphi/v_K$), and (c) $\sqrt{c_3}$ ($= c_s/v_K$). The solid curves are for the case of the present critical disk with mass loss ($s = 1/2$), whereas the dashed ones are for the case of the supercritical disk without mass loss ($s = -1/2$). The values of α are 0.1, 0.5, and 1. The ratio of specific heats is set to be $\gamma = 4/3$.

When s is $-1/2$, these expressions reduce to those found by Narayan and Yi (1994).

The parameters of the model are the ratio of the specific heats γ, the standard viscous parameter α, and the energy-advection fraction f.

Comparing the case without mass loss ($s = -1/2$) and the case with mass loss ($s > -1/2$), for $s > -1/2$, ϵ' decreases and f increases. Hence, the effect of mass loss is similar to the advection effect.

These parameter c_i's are shown in figure 6 as a function of the advection factor f for several values of the viscous parameter α. The solid curves are for the case of the present critical disk with mass loss ($s = 1/2$), whereas the dashed ones are for the case of the supercritical disk without mass loss ($s = -1/2$). The values of α are 0.1, 0.5, and 1. The ratio of specific heats is set to be $\gamma = 4/3$.

A.3. Radiation Properties

The surface flux and disk luminosity of the supercritical model are derived as follows.

By assuming a dominance of the radiation pressure, we can write the height-integrated pressure Π ($= \Sigma c_s^2$) and the averaged flux F as

$$\Pi = \Pi_{\rm rad} = \frac{1}{3} a T_c^4 2H = \frac{8H}{3c}\sigma T_c^4, \tag{A18}$$

$$F = \sigma T_c^4 = \frac{3c}{8H}\Pi = \frac{3}{8} c\Sigma_0\sqrt{c_3} G M r^{s-2}, \tag{A19}$$

where σ is the Stefan–Boltzmann constant. The optical thickness of the disk in the vertical direction is

$$\tau = \frac{1}{2}\kappa\Sigma = \frac{1}{2}\kappa\Sigma_0 r^s, \tag{A20}$$

where κ is the electron-scattering opacity.

Hence, the effective flux and the effective temperature of the disk surface become

$$\sigma T_{\rm eff}^4 = \frac{\sigma T_c^4}{\tau} = \frac{3c}{4\kappa}\sqrt{c_3}\frac{GM}{r^2} = \frac{3}{4}\sqrt{c_3}\frac{L_E}{4\pi r^2}, \tag{A21}$$

It should be emphasized that the radiative appearance, such as $T_{\rm eff}$, are not affected by the mass loss, although the pressure Π and the averaged flux F depend on the mass-loss distribution. This can be understood as follows. When there is a wind mass loss from the disk surface, the averaged flux F decreases all over the disk, compared with the no-wind case. At the same time, the surface density and optical depth decrease for the mass loss case, compared with the no-wind case. That is, we see the deep inside of the disk in the case with mass loss. As a result, the effective temperature of the disk does not depend on the mass loss, and the radiative appearance is similar to that without mass loss.

A.4. Accretion Rates

Using the self-similar solutions, the mass-accretion rate is expressed as

$$\dot{M} = -2\pi r\Sigma v_r = \dot{M}_{\rm input}\left(\frac{r}{r_{\rm out}}\right)^{s+1/2}, \tag{A22}$$

where $r_{\rm out}$ is the radius of the disk outer edge and $\dot{M}_{\rm input}$ is

the accretion rate there. In the critical accretion disk, $r_{\rm out}$ is replaced by the critical radius $r_{\rm cr}$.

Because of the critical condition (6), we have imposed, for the inner critical disk, that the mass-accretion rate should be $\dot{M} \propto r$ in the inner critical region; therefore, the parameter s is fixed as $s = 1/2$.

References

Abramowicz, M. A., Chen, X., Kato, S., Lasota, J.-P., & Regev, O. 1995, ApJ, 438, L37

Abramowicz, M. A., Czerny, B., Lasota, J. P., & Szuszkiewicz, E. 1988, ApJ, 332, 646

Begelman, M. C. 1979, MNRAS, 187, 237

Beloborodov, A. M. 1998, MNRAS, 297, 739

Bisnovatyi-Kogan, G. S., & Blinnikov, S. I. 1977, A&A, 59, 111

Boller, Th., Brandt, W. N., & Fink, H. 1996, A&A, 305, 53

Eggum, G. E., Coroniti, F. V., & Katz, J. I. 1988, ApJ, 330, 142

Fukue, J. 1996, PASJ, 48, 89

Fukue, J. 2000, PASJ, 52, 829

Hirai, Y., & Fukue, J. 2001, PASJ, 53, 285

Ichimaru, S. 1977, ApJ, 214, 840

Icke, V. 1980, AJ, 85, 329

Icke, V. 1989, A&A, 216, 294

Kato, S., Fukue, J., & Mineshige, S. 1998, Black-Hole Accretion Disks (Kyoto: Kyoto University Press)

Katz, J. I. 1980, ApJ, 236, L127

King, A. R., & Begelman, M. C. 1999, ApJ, 519, L169

Kitabatake, E., & Fukue, J. 2003, PASJ, 55, 1115

Kitabatake, E., Fukue, J., & Matsumoto, K. 2002, PASJ, 54, 235

Kubota, A. 2001, PhD Thesis, The University of Tokyo

Melia, F., & Königl, A. 1989, ApJ, 340, 162

Mineshige, S., Kawaguchi, T., Takeuchi, M., & Hayashida, K. 2000, PASJ, 52, 499

Mirabel, I. F., & Rodríguez, L. F. 1998, Nature, 392, 673

Narayan, R., & Yi, I. 1994, ApJ, 428, L13

Ohsuga, K., Mineshige, S., Mori, M., & Umemura, M. 2002, ApJ, 574, 315

Ohsuga, K., Mineshige, S., & Watarai, K. 2003, ApJ, 596, 429

Popham, R., & Gammie, C. F. 1998, ApJ, 504, 419

Shakura, N. I., & Sunyaev, R. A. 1973, A&A, 24, 337

Szuszkiewicz, E., Malkan, M. A., & Abramowicz, M. A. 1996, ApJ, 458, 474

Tajima, Y., & Fukue, J. 1996, PASJ, 48, 529

Tajima, Y., & Fukue, J. 1998, PASJ, 50, 483

Watarai, K., & Fukue, J. 1999, PASJ, 51, 725

Watarai, K., Fukue, J., Takeuchi, M., & Mineshige, S. 2000, PASJ, 52, 133

Watarai, K., & Mineshige, S. 2003, ApJ, 596, 421